



Published in final edited form as:

*J Nanopart Res.* 2016 October ; 18(10): . doi:10.1007/s11051-016-3328-y.

## Surface-initiated ring-opening metathesis polymerization (SI-ROMP) to attach a tethered organic corona onto CdSe/ZnS core/shell quantum dots

**Fatma Vatansever** and

Wellman Center for Photomedicine, Massachusetts General Hospital, Boston, MA 02114, USA.  
Department of Dermatology, Harvard Medical School, Boston, MA 02115, USA

**Michael R. Hamblin**

Wellman Center for Photomedicine, Massachusetts General Hospital, Boston, MA 02114, USA.  
Department of Dermatology, Harvard Medical School, Boston, MA 02115, USA. Harvard-MIT  
Division of Health Sciences and Technology, Boston, MA 02139, USA

### Abstract

Core-shell CdSe/ZnS quantum dots (QDs) are useful as tunable photostable fluorophores for multiple applications in industry, biology, and medicine. However, to achieve the optimum optical properties, the surface of the QDs must be passivated to remove charged sites that might bind extraneous substances and allow aggregation. Here we describe a method of growing an organic polymer corona onto the QD surface using the bottom-up approach of surface-initiated ring-opening metathesis polymerization (SI-ROMP) with Grubbs catalyst. CdSe/ZnS QDs were first coated with mercaptopropionic acid by displacing the original trioctylphosphine oxide layer, and then reacted with 7-octenyl dimethyl chlorosilane. The resulting octenyl double bonds allowed the attachment of ruthenium alkylidene groups as a catalyst. A subsequent metathesis reaction with strained bicyclic monomers (norbornene-dicarbonyl chloride (NDC), and a mixture of NDC and norbornylethylisobutyl-polyhedral oligomeric silsesquioxane (norbornoPOSS)) allowed the construction of tethered organic homo-polymer or co-polymer layers onto the QD. Compounds were characterized by FT-IR, <sup>1</sup>H-NMR, X-ray photoelectron spectroscopy, differential scanning calorimetry, and transmission electron microscopy. Atomic force microscopy showed that the coated QDs were separate and non-aggregated with a range of diameter of 48–53 nm.

### Keywords

Tunable fluorophores; Nanomaterials; Quantum dot; Surface functionalization; Surface-initiated ring-opening metathesis polymerization; Grubbs catalyst; Nanomedicine

### Introduction

With the ever-increasing demand for new fluorescent materials as fluorescent labels/sensors that may also incorporate flexibility, high-temperature proton-conducting components, oxygen stability, etc. require developing innovative approaches to tailor sought-after physicochemical and optical properties. Advances in the preparation of high-quality nanometer-size semiconductor crystals (Alivisatos 2001; Dabbousi et al. 1997; Danek et al.

1996; Guyot-Sionnest and Hines 1998; Peng et al. 2000; Tian et al. 1996) known as quantum dots (QDs) now allow tailoring the optical properties and quantum effects arising from the size variations with other desired properties applicable in a broad technological range.

However, large surface-to-volume ratio of the QDs implies that the surface that contains many atoms with uncoordinated valences is the dominant factor in causing uncontrolled variability in optical properties. Complete and controlled passivation of these cationic and anionic sites at the surface is critical. Growing inorganic shells around the core, which exhibit low defect density, lattice-matched interfaces, and an electronic band gap larger than that of the core, leads to environmentally stable, core-shell QDs with increased luminescence and quantum yields (Talapin et al. 2001). Functionalization of the core-shell QDs, on the other hand, enables incorporation/integration of the QDs into a system that provides additional sought-after properties. Thus, developing feasible techniques for controlled surface functionality of the QDs is critical for facile processing and the ability to pattern, chemically attach, and spatially arrange QDs on various substrates, including metallic, ceramic, polymeric, semiconductor, and biological materials. Furthermore, the unique properties of organic polymers and the importance of the organic-inorganic interface for optimum performance necessitate continual development of alternative techniques for growth, deposition, control, and manipulation of a tethered, organic layer (Hasan et al. 2002; Shipway and Willner 2001; Skaff et al. 2002). Thus, far developments in this direction lead to the rapid proliferation of solution-synthesized QDs to be incorporated in nanoelectronic (Bao and Bawendi 2015; Duan et al. 2001; Fuhrer et al. 2000; Gudiksen et al. 2002), optoelectronic (Fan et al. 2015b; Ganesh et al. 2007; Labelle et al. 2015; Nasilowski et al. 2015; Sun et al. 2015), and biomedical (Alivisatos 2004; Banerjee et al. 2015; Bhana et al. 2015; Cao et al. 2014; Chan and Nie 1998; Chen et al. 2015; Cho 2015; Feugang et al. 2015; Wang et al. 2015; Zhang and Zhao 2014; Zhang and Wang 2012) applications with both active and passive targeting (Cho 2015).

Organic-inorganic interfacing can be achieved by two approaches: top-down (convergent) or bottom-up (divergent), preference depending on the application and structure of the macromolecular corona (size, composition, and density). Top-down approaches (Dawson and O'Riordan 2014; Diaz Fernandez et al. 2014; Fan et al. 2015a; Jiang et al. 2014; Lalatsa and Serrano Lopez 2015; Wijesena et al. 2015) are typified by the attachment of pre-synthesized macromolecular units; however, steric repulsion and crowding at the surface limit the attachment density, as the molecular weight of the macromolecular unit increases. Bottom-up approaches (Diaz Fernandez et al. 2014; Lalatsa and Serrano Lopez 2015; Tenenbaum et al. 2015; Zhao and Liu 2015) are typified by sequential attachment of reactive moieties to the interfacial region, resulting in growth of the organic unit from the interface outwards (Levicky et al. 1998; Samanta et al. 2015). This approach provides ultra-high density of functionalization and could in principle allow exquisite spatial and compositional control. However, the need for purification after each step, and the possible detrimental influence of the surface on chemical reactions could be problematic. Recently, surface-initiated polymerization (SIP) reactions (Islam et al. 2014; Lei et al. 2014; Wang et al. 2011) have been demonstrated to occur on various forms of solid substrates (bulk surface, powders, and nanoparticles) composed of gold (Yenice et al. 2015), silica (Prucker and Ruhe 1998a; Prucker and Ruhe 1998b; Schneider et al. 2013), or fumed silica (Hou et al. 2010).

In this work, we describe the synthesis and functionalization of core/shell CdSe/ZnS QDs via surface-initiated ring-opening metathesis polymerization (SI-ROMP) using cyclic strained monomers. We demonstrate the ability to control composition, architecture, and molecular weight of the developed macromolecular corona. The process involves modification of the organic-ligand layer tri-octylphosphine oxide (TOPO) to produce core/shell QDs with “active” sites, consisting of surface-tethered ruthenium alkylidene complexes. This robust and highly reactive catalyst enabled growth of homo-polymers and copolymers, in a controlled manner, directly from the QD surface.

## Results and discussion

Figure 1 illustrates the reaction schemes involved in the controlled growth of a macromolecular corona onto QD using SI-ROMP.

To tailor the QDs' surface, it is necessary to exchange the TOPO, present in the synthesis medium as a coordinating ligand, with a substrate that exhibits a higher binding potential as well as possessing the desired functionality. The catalyst to be used for polymerization from the surface must be robust and highly reactive with balanced electronic and coordinative unsaturation. Previous efforts have shown that a ruthenium alkylidene complex (Nguyen et al. 1992, 1993; Walba et al. 1996; Wu et al. 1995) is catalytically active in the presence of a wide range of functional groups (Grubbs 1994), such as halogens (Schwab et al. 1996), hydroxyl groups (Schwab et al. 1996), aryl esters (Walba et al. 1996), nitro groups (Walba et al. 1996), ketones, and aldehyde functionalities (Nguyen et al. 1993). Additionally, carboxylic acids and carbonyl groups (Crimmins and King 1996) do not affect the catalytic activity and perform well even in aqueous media (Lynn et al. 1996); thus, ruthenium alkylidene could be an excellent choice to develop a general methodology for QD functionalization. In our strategy, we had sequestered the ruthenium at the distal end of the organic corona while using an exchange ligand with a terminal double bond. Careful manipulation of the reaction conditions facilitated a successful metathesis reaction producing an active catalyst tethered to the QD surface. This in return provided a handle for growing the polymer from strained bicyclic monomers directly from the surface. The following sections will discuss the various steps outlined in Fig. 1.

### Nanocrystal synthesis

The semiconductor QDs that are being used for biological/cellular studies' applications due to their synthesis technique lack sharpness and tunability of emission as well as long-term stability due to increased number of defects in the crystal lattice inherent for various synthesis techniques proposed in replacing the inherently dangerous original synthesis technique of decomposing the precursors in hot coordinating solvents and then initiate the crystal lattice formation anew. Our goal was to synthesize CdSe QDs that mimic the original-“true” QD synthesis technique that is providing excellent control over the particle growth kinetics and crystal lattice formation and, thus, of the optoelectronic properties. However, purification of  $\text{Cd}(\text{CH}_3)_2$  by vacuum distillation is tedious and inherently dangerous process, thus we employed an alternative purification method of the precursor and evaluated the optical properties of the resulting CdSe QDs.

In the study, the CdSe and CdSe/ZnS QDs were prepared by the well-established synthetic technique of decomposing organometallic precursors in coordinating solvent(s) at elevated temperatures (Alivisatos 1996b, 2001; Manna et al. 2000; Peng et al. 2000). It is known that semiconductor nanocrystals exhibit size-tunable optical properties, due to the confinement of the electronic wave function, where optical transition of the first excitonic state and the electronic levels, as a norm, shift with increasing particle size (Ekimov et al. 1993; Hines and Guyot-Sionnest 1996; Katari et al. 1994; Murray et al. 1993; Peng et al. 1997; Weller 1993), i.e., the discrete density of state gap (with the Fermi level lying between HOMO–LUMO bands) decreasing by increasing the nanocrystal size (Alivisatos 1996a). This phenomenon is clearly visible in Fig. 2a. In our study, we employed the already-established synthesis approach that separates the crystal nucleation from growth by injecting rapidly and at high temperature the core components (to induce nucleation) and then reducing the temperature during the growth phase; a process that critically depends on the kinetics of the initial nucleation, thus purity of precursors (Katari et al. 1994; Manna et al. 2000; Peng et al. 1998; Peng et al. 2000). This approach clearly allows better control over the Fermi energy levels, thus the absorption wavelengths.

The crystal size evolution of the cores was carefully monitored via UV–vis spectroscopy through constant sampling of the reaction media by taking aliquots with Fig. 2a comparing the UV–vis spectra of CdSe QDs synthesized using filtered, vacuum-distilled, and as-received Cd(CH<sub>3</sub>)<sub>2</sub> precursor. As anticipated, the vacuum-distilled precursor yielded QDs with the finest control over the energy states, demonstrated by narrow and highly resolved absorption peaks. As-received Cd(CH<sub>3</sub>)<sub>2</sub> provided poor size evolution control and poor optical quality. Surprisingly, the optical footprint of CdSe QDs with only filtered material was similar to that from vacuum distilled. However, the size evolutions after secondary injections were hard to control.

Unfortunately, TOPO-coated CdSe QDs are unstable to photooxidation (Alivisatos 1996a); thus, effective passivation of CdSe core is required. QD surface passivation is a chemical process by which the core surface atoms are bonded to another material (with much larger band gap) to eliminate all energy levels inside the gap, and this can be achieved in two ways. The first one is via a disordered material accommodating core's local bonding geometry, as is the case with a component of the initial coordinating solvent of the high-temperature reaction, the TOPO; proven to be effective in passivating the CdSe surface through the phosphine oxide sites, interacting with the Cd atoms at the surface (Alivisatos 1996a; Guzelian et al. 1996). The second approach is via epitaxial growth of shell layer(s), where the crystal structures and bond lengths of the two materials do match and generate core/shell construct that is optoelectronically more stable over extended lifetime. In our study, the stable and long-time effective electronic passivation of the CdSe core is achieved by ZnS shell “build up” (Hines and Guyot-Sionnest 1996; Klimov et al. 1999; Nirmal and Brus 1999; Peng et al. 1997; Talapin et al. 2001) where the epitaxial growth of the ZnS shell, i.e., core surface passivation effects, is monitored via an established PL (emission) evolution. The ZnS was a choice of shell component since it is proven to have compatible lattice structure and deposition chemistry with CdSe as well as larger band gap (Manna et al. 2000; Pancove 2010; Peng et al. 2000). The PL results of the study indicate that our core/shell synthesis method of ZnS-passivated CdSe cores exhibits enhanced fluorescence, which is in

agreement with previously reported studies (Danek et al. 1996; Hines and Guyot-Sionnest 1996; Peng et al. 1997). Moreover, the synthetic conditions described allow for good control over shell thickness growth, thus photoluminescence. Figure 2b compares the photoluminescence (PL) spectra of ZnS shell evolution on CdSe cores from filtered  $\text{Cd}(\text{CH}_3)_2$  where the increase in the luminescence in CdSe with shell growth demonstrates an effective electronic passivation of the CdSe dots with added ZnS overlayer(s). A red shift in the first excited state ( $1s_e-1s_h$ ) occurs with formation of the ZnS shell due to lowering of the localization energy of the electrons (Dabbousi et al. 1997; Heath and Shiang 1998; Klimov et al. 1999) whose wave function extends into the shell region. The improved photoluminescence also qualitatively demonstrates that the epitaxial growth of higher-band gap inorganic shell of ZnS passivates the non-radiative recombination sites at the surface (Islam et al. 2014). We observed a 10 % increase in the quantum yield of core/shell CdSe/ZnS in comparison with CdSe cores, 9.4 and 0.2 %, respectively. The TEM micrographs displayed in Fig. 2c, d show uniform-sized QDs with narrow size distribution with lattice parameters measured directly off the micrograph negatives and that are consistent with published distilled precursors' synthesized CdSe and CdSe/ZnS QDs (Alivisatos 1996a; Peng et al. 1997). Moreover, our observations regarding surface constituents, optoelectronic properties, and surface studies all are consistent with previous reports of QDs generated using vacuum-distilled  $\text{Cd}(\text{CH}_3)_2$  precursors.

### Ligand exchange

To facilitate ligand exchange, we first had to remove the excess TOPO. At least four washing steps of CdSe/ZnS QDs with MeOH were necessary to produce core/shells with an approximate single monolayer of TOPO. This monolayer was subsequently displaced from the QD surface with mercaptopropionic acid using mass action, where a fresh addition of mercaptopropionic acid was added daily for 4 days. NMR and FT-IR provided spectroscopic verification of the presence of surface-associated TOPO and subsequent exchange with mercaptopropionic acid.

The FT-IR of the QDs before ligand exchange indicated the presence of surface-bound TOPO evident from the shift in the P–O stretching frequency (from 1145 to 1090  $\text{cm}^{-1}$ ) due to lowering of stretching energy upon complexation; since there is a transfer of electron density from P to O, P becomes more positive when “complexed to” Cd. The comparison of unbound with surface-bound TOPO reveals shift as well as change in the shape of the resonating protons with proton NMR study. The effect of the semiconductor QDs on surface-attached TOPO is pronounced even at the distal  $\text{CH}_3$  protons, which appear to resonate downfield in the range of 0.96–0.888 with a very different splitting pattern. The presence of the bump, an indication of restriction in the proton motion, at 1.67–1.378 is an additional evidence for having TOPO chemically attached to the ZnS shell surface.

After the exchange with mercaptopropionic acid, the characteristic absorption peaks associated with TOPO were replaced by those from mercaptopropionic acid, Fig. 3a. Surface association of the acid was indicated by the absence of S–H absorption (at 2676 and 2565  $\text{cm}^{-1}$ ) as well as the shifting of the carbonyl stretching peak from 1713  $\text{cm}^{-1}$  to 1630 and 1560  $\text{cm}^{-1}$ , with a change in the peak shape as well giving a clear indication of a change in

environment. Also the S–CH<sub>2</sub> wagging absorption is observed at 1384 cm<sup>-1</sup>. Furthermore, the O–H stretching absorption peak becomes sharper and more pronounced, indicating that H-bonding in the acid was reduced after the surface attachment.

The proton NMR corroborates the FT-IR evidence for the exchange of surface-associated TOPO (Fig. 3b) with mercaptopropionic acid (Fig. 3c). The downfield shift and broadening in the carbonyl-attached CH<sub>2</sub> protons (see the splitting pattern) arising from the effect of the metallic core provide additional evidence of surface attachment. Furthermore, protons from the CH<sub>2</sub> next to the S resonate downfield (2.83 to 2.68δ) with completely disturbed splitting pattern. In the proton NMR of free mercaptopropionic acid, with the O–H proton resonating at 11.7δ, since essentially every OH proton is H-bonded, the acid protons resonate at very high frequency, i.e., downfield. The two protons of CH<sub>2</sub> attached to the carbonyl group resonate in the 1.68–1.61δ range and appear as a triplet (in accordance with the chemical structure). S–H protons and protons of CH<sub>2</sub> next to S appear in the 2.75–2.63δ range as multiplet with a splitting pattern in exact accordance with the structure of the molecule.

### Catalyst sequestering

Mercaptopropionic acid exchange provided a flexible surface functionality for subsequent attachment of organic and inorganic reactants, such as sequestering of the ruthenium alkylidene complex, required for creating “active” sites on the QD surface. After repeated washing of the mercapto-exchanged QDs with dry hexanes to remove the unreacted acid, terminal double bonds were created with 7-octenyl dimethyl chlorosilane. This is a typical nucleophilic elimination reaction at an Si center with high efficiency that reaches completion almost instantly. The formation of the organic layer of terminal double bonds attached to the QD surface was verified both by FT-IR and NMR. Completion of the reaction and the presence of octenyl silane groups on the surface were demonstrated by the peaks of Si–O stretching (1095, 1026, and 800 cm<sup>-1</sup>) as well as Si–C stretching at 1263 cm<sup>-1</sup>. Moreover, the carbonyl stretching absorption shifted to 1655 cm<sup>-1</sup>, Fig. 4a. Proton NMR verified the octenyl silane attachment to the mercapto acid-modified QD surface. The absence of a resonance shift in –Si–(CH<sub>3</sub>)<sub>2</sub>– protons, due to Cl effect, is a clear evidence that the octenyl silane reacted with the acid end of the mercaptopropionic acid, Fig. 4b. After the attachment, the –Si–(CH<sub>3</sub>)<sub>2</sub>– protons resonated at 0.32–0.05δ range. It is known that in unreacted 7-octenyl dimethyl chlorosilane the Cl–Si–(CH<sub>3</sub>)<sub>2</sub>– protons resonate in the 0.42–0.39δ region. If there was no chlorine attached to the Si, the –Si–(CH<sub>3</sub>)<sub>2</sub>– protons would have resonated at 0.00–0.01δ (as it is in the case of TMS (tetra-methyl silane) where the Si(CH<sub>3</sub>)<sub>4</sub> protons resonate at 0.00δ). After surface attachment, since the chlorine is eliminated (i.e., there is no chlorine effect), the –Si–(CH<sub>3</sub>)<sub>2</sub>– protons are shown to resonate at 0.32–0.05δ region and this constitutes a proof that surface attachment took place indeed.

The most compelling evidence for attachment of the catalyst to the QD surface came from <sup>1</sup>H NMR studies. The alkylidene proton in the pristine catalyst resonated at 20.62δ. After surface attachment, the same proton resonated at 19.90δ due to the change in its environment, Fig. 4c.

The use of a two-step procedure to create terminal double bonds at the QD surface may appear redundant; however, by separating the ligand exchange from the surface

functionalization and catalyst attachment, flexibility in the synthetic design is maximized. In addition, this approach provides good control over the spatial density of the active catalyst, by utilizing “spacers” to keep the active sites apart. These spacers are organic moieties that can be sequestered to the QD surface at one end, while the free end does not have a double bond.

These QD surface-tethered terminal double bonds were used to metathesize the ruthenium alkylidene catalyst. The use of an organometallic catalyst for growing polymer from the semiconductor QD surface has two advantages: firstly, polymer chains can grow only from the catalyst-attached sites. The second advantage is that it provides better control over the polymer chain length, since the catalyst is chemically attached to the surface and the polymer grows between that surface and the catalyst at the distal end (Dias et al. 1997). Olefin metathesis is described as a catalytic process with formation of an unstable [2 + 2] addition product giving a four-membered metallacyclic ring between the olefin and the transition metal complex acting as an intermediate (Ivin and Mol 1997). The collapse of the metallacycle can give either the products and/or the original reactants. In that respect, the reaction conditions are very important in order to push the reaction toward products. Initially, the dichloromethane-dissolved catalyst and QDs were kept in separate vials at  $-10\text{ }^{\circ}\text{C}$ . After mixing the two solutions, the color changed from purple (that of the original catalyst solution) to brown, a reflection of a change in the environment of the Ru-alkylidene, indicating attachment of the catalyst to the QD surface via metathesizing through distal terminal double bonds.

Surface-sensitive XPS provided qualitative evidence that the Ru catalyst was attached to the QD surface. Both survey (Fig. 4d) and high-resolution scans revealed the presence of Ru  $3p_{1/2}$ ,  $3p_{3/2}$ ,  $5d_{5/2}$  (Fig. 4e) as well as C (Fig. 4f), and Si (Fig. 4g).

Although each step in these processes was highly efficient, the number of synthetic steps and the numerous washing steps in between resulted in  $\sim 70\%$  yield of modified QD material ready to undergo polymerization.

### SI-ROMP (surface-initiated ring-opening metathesis polymerization)

The SI-ROMP was applied successfully to grow both a homo-polymer using norbornene-dicarbonyl chloride (NDC) (trans-3, 6-endomethylene-1, 2, 3, 6-tetrahydrophthaloylchloride) as well as a co-polymer of the combination of NDC with norbornenylethylisobutyl-POSS (norbornoPOSS) from the CdSe/ZnS QD surface. NorbornoPOSS was chosen as one of the monomers to be used due to its precise three-dimensional structure providing a molecular-level reinforcement of polymer segments and coils, in addition to improving physical and thermal properties of polymer systems, where the presence of silicon–oxygen linkage generates polymers with extended temperature ranges, reduced flammability, lower thermal conductivity, and resistance to atomic oxygen.

In the SI-ROMP system, the polymerization occurs by the insertion of the monomer between the modified QD and ruthenium catalyst. Since growth points are fixed and surface attached, there is practically no polymerization in the bulk material. The catalyst operates via the so-called “dissociative pathway” with metallacycle formation being the rate-determining step

(Dias et al. 1997). ROMP can be considered as a “living” process with respect to the rate of monomer consumption, i.e., the polymerization continues until the monomer is consumed and resumes again upon subsequent addition of more monomer. This process provides better control over the molecular weight distribution and polydispersity of the final product.

Real-time polymerization of the NDC monomer onto Ru-attached QDs in *d*-chloroform was monitored in situ via proton NMR spectroscopy where peaks due to polymer formation began to emerge in the first 5 min of the polymerization reaction. After 5 hours, the monomer was almost completely converted to polymer, as evident from Fig. 5a, with the last measurements showing all the characteristic peaks due to the polymer growth from the surface. We observed that with time (around 10–15 min) the viscosity of the reaction medium increased reaching a point where it was impossible for the stir bar to agitate the reaction mixture.

The same synthetic method was applied to grow copolymers of NDC with norbornoPOSS from the QD surface by simultaneous addition of both monomers. The presence of the two components in the final product was substantiated by IR. From the norbornoPOSS component, a broad and intense peak at  $1101\text{ cm}^{-1}$  (due to the asymmetric Si–O–Si stretching), two Si–O–Si absorptions at  $742$  and  $480\text{ cm}^{-1}$ , and the characteristic *geminal*-dimethyl splitting pattern (due to the presence of *i*-butyl from the R groups of the cage) appearing at  $1465$  and  $1436\text{ cm}^{-1}$  were observed. All these features were observed in free polymerized copolymer as well. From the norbornene-dicarbonyl ester (NDE) component, the presence of carbonyl group was manifested by the very strong and sharp peak at  $1735\text{ cm}^{-1}$ , Fig. 5b. Taking into consideration the bulkiness of the POSS cage, the copolymerization reaction time was extended to 24 h although the reaction conditions were kept the same as for the homo-polymer synthesis.

A final work-up was required after the polymerization process was over. This involved precipitating the polymer in ice-cold MeOH in order to get rid of any unreacted monomer as well as separating the polymer from the reaction medium. Meanwhile, the carbonyl chloride groups at the ends get converted to methyl esters. The polymer chain ends are still “active,” since the catalytic activity of the ruthenium catalyst is not altered, and so after completing the polymerization process these ends need to be sealed off. This is achieved by an “end-capping” process, where the active catalyst is removed from the polymer chain ends as well as the desired end-group functionalization was obtained.

A control reaction of attempted polymerization of NDC and norbornoPOSS monomers on the QD surface prior to catalyst attachment did not yield any polymer.

### Characterization and morphology

Table 1 summarizes the physical characteristics of the polymers recovered from the QD surface and free-grown homo-polymers and co-polymers.

Thermal analysis studies confirmed the formation of QD surface-grown homo-polymers and co-polymers. The glass transition temperature ( $T_g$ ), as determined from the second heating scan, confirmed the expectation that  $T_g$  increased with increasing polymer chain length of

both recovered and free-grown polymers. The observed substantial increase in the T<sub>g</sub> of norbornene-dicarbonyl ester (NDE) was due to the fact that there were polar groups in the linear polymer backbone; in fact, there are two –OCH<sub>3</sub> groups per monomer unit. Polar interactions between neighboring chains cause the T<sub>g</sub> to rise, so that short- and long-chain NDE polymers have different T<sub>g</sub> values. When compared with the reported T<sub>g</sub> value for unsubstituted polynorbornene (T<sub>g</sub> ~55 °C), one can appreciate the polar group effect on the glass transition behavior. Also, the change in T<sub>g</sub> of the random linear hybrid co-polymer with integrated norbornoPOSS units can be also attributed to the fact that norbornoPOSS (as an integral part of the co-polymer) forms aggregates of nanometer-sized flexible cylinders and/or spheres. Thermal studies revealed that QD-grown and free-grown polymers had similar thermal characteristics. The effects of chain length and polar group were clearly attributed to the polymer chains from both systems.

### Morphology studies

AFM imaging was used to show the lack of aggregation in QD with polymer coronas grown from the surface. QD-grown NDE versus free-grown NDE showed distinctive features, Fig. 5c, d. In the QD-grown polymer, there was noticeable separation and dispersion in the monolayer with spheres exhibiting a nominal diameter of 40 ± 5 nm with no preferential ordering, whereas the free-grown polymer did not demonstrate any segregation or dispersion when cast into a thin film. The two films were annealed at 80 and 120 °C for 10 min and imaged with the AFM after each annealing. There was no noticeable change in morphology of the cast films upon annealing.

The AFM showed spherical features (globules) for the NDE polymer grown from the CdSe/ZnS surface, which were evaluated further by comparing the volumes of the pristine QD with the total volume of the globules. If the total volume of the globules comprises the sum of the volume of the CdSe/ZnS QD and the volume of the grown polymer, the total volume of that globule can be expressed as V<sub>QD+organic corona</sub> and the volume ratios can be expressed as

$$V_{\text{QD+org. corona}}/V_{\text{QD}} = (R_{\text{QD}} + R_{\text{org. corona}})^3 / R_{\text{QD}}^3.$$

## Experimental

### Instrumentation

**Spectroscopy**—FT-IR spectra were collected using a Thermo Nicolet NEXUS 470, as standard KBr pellets and solutions from KBr window. NMR spectra were collected with VARIAN 200 and Bruker with 300 MHz and 250 MHz fields, respectively. UV–vis absorption spectra were obtained by Shimadzu MultiSpec 1500 with 512-element diode array spectrometer and xenon–deuterium lamp source. Photoluminescence experiments were conducted on a Shimadzu RF-5301PC spectrofluorophotometer with collection at 90° and a resolution of 1.5 nm. Quantum yield (QY) measurements were done with Rhodamine 6G dye used as a reference. X-ray photoelectron spectroscopy (XPS) was performed on a

Surface Science M Probe Surface Spectrometer with an X-ray source of Al K $\alpha$  (1486.6 eV). Dilute solution of the QDs in chloroform was applied with a pipette on the silicon wafer. Survey and high-resolution spectra were obtained from 1000  $\times$  400 nm area (450–500 and 270–290 eV). Sweeping rates were 1–2 eV/step with a dwell time of 200 ms and the number of scans from 4 to 10. Sputtering with argon was not performed in order to observe the presence of the ruthenium catalyst at the surface termini.

**Morphology**—TEM was performed on Philips CM 200 FEG. Samples were prepared by placing a drop of dilute solution of the QDs in toluene onto 50-Å-thick carbon-coated copper grids (400 mesh) where the excess solution was immediately removed via a paper napkin. AFM imaging was performed on Digital Instruments Veeco Metrology Group Dimension 3100 Atomic Force Microscope with a Nanoscope IIIa controller in tapping mode. Dilute solutions of QD-NDE and free-NDE were placed on a silicon wafer. Once a razor blade was used to make a scratch in order to have a height reference to the silicon substrate.

**Thermal analysis**—Differential scanning calorimetry (DSC) data were collected with TA Instrument DSCQ1000. Temperature increments were 10 °C/min and nitrogen purge of 50 ml/min. The scans were done in two cycles: initial scan and rescan after reaching 200 °C. TGA data were collected with a TA Instrument TGA2950. Temperature increments were 10 °C/min with 50 ml/min purging with He.

GPC data were collected with Waters 150-C ALC/GPC ultra-styragel system combined with ultraviolet and diffractive index detectors.

## Chemicals

Anhydrous MeOH, anhydrous toluene, anhydrous dichloromethane, pentane, trans-3,6-endomethylene-1,2,3,6-tetrahydrophthaloylchloride (97 %), 3-mercaptopropionic acid (99+ %), and hexamethyldisilathiane ((TMS)<sub>2</sub>S) were purchased from Aldrich and used without further purification. TOPO (90 % purity) was purchased from Alfa Aesar. Tri-*n*-butyl phosphine (TBP, 99 %), bis(tricyclohexylphosphine)benzylidene ruthenium(IV) dichloride, and dimethylcadmium (Cd(CH<sub>3</sub>)<sub>2</sub>, 97 %) were purchased from Strem Chemicals. Selenium (Se, 99.999 % purity) 100-mesh powder and diethylzinc (Et<sub>2</sub>Zn, 1.0 M solution in heptane) were purchased from Aldrich. Both Cd(CH<sub>3</sub>)<sub>2</sub> and Et<sub>2</sub>Zn were filtered through an array of 0.2–0.1–0.05  $\mu$ m pore size filters prior to use. 7-octenyl dimethyl chlorosilane was purchased from Gelest. Norbornenylethylisobutyl-POSS<sup>®</sup> (norbornoPOSS) was procured from Hybrid Plastics. Rhodamine 590, for QY measurements, was purchased from Exciton.

## Stock solutions

All stock solutions for the core and core/shell quantum dots were prepared in a dry box under N<sub>2</sub> atmosphere and kept refrigerated at –18 °C.

Stock solution for CdSe was prepared as follows: in a vial, 0.147 g of powder Se was dissolved completely in 9.48 g TBP to which 0.371 g of Cd(CH<sub>3</sub>)<sub>2</sub> was added (i.e., Se-to-Cd

ratio was kept at 2:3). A septum was attached atop and the vial was taken out of the dry box to be chilled out for an hour prior to use.

Stock solution for ZnS was prepared as follows: in a vial, 3.30 g of TBP, 0.36 g (TMS)<sub>2</sub>S, and 1.26 g Et<sub>2</sub>Zn were mixed. The whole system was further diluted with 4.89 g TBP. A septum was attached atop the vial after which it was taken out of the dry box and placed in a refrigerator at -18 °C to chill out for an hour prior to use.

## Syntheses

**CdSe core synthesis**—A tri-neck flask of 25 ml volume, equipped with a stir bar, was charged with 4 g TOPO. Vacuum was applied while temperature was raised to 120 °C and kept there for about an hour. Vacuum was turned off, the Ar purge initiated along with an increase in temperature in small increments, and finally the temperature was stabilized at 360 °C (under constant Ar flow and vigorous stirring). Prior to injecting the core components, the syringe–needle system was flushed a couple of times with air after which 2 ml of the CdSe stock solution was rapidly injected. At that point, the temperature of the reaction media fell by 60 to 70 °C, on average. The temperature was stabilized at 300 °C during the crystal growth. The reaction was quenched by removing the heating mantle and injecting 5 ml of anhydrous MeOH before the temperature fell to below 40 °C. The CdSe nanocrystals precipitated after the addition of the MeOH and were separated via centrifugation. The precipitate was washed three times with dry MeOH in 5 ml portions, dried under an Ar flush, and kept under an inert atmosphere. Aliquots at different stages of the crystal growth were taken for analysis.

**CdSe/ZnS core/shell synthesis**—A tri-neck flask, equipped with a stir bar, was charged with 4 g TOPO. Vacuum was applied while the temperature was raised to 120 °C and kept there for about an hour with vigorous stirring. The vacuum was turned off and the Ar purge began while lowering the temperature to 50 °C at which point 35.4 mg CdSe core material, dissolved in 2 ml dry pentane, was introduced into the reaction flask. Vacuum was applied and the temperature rose in small increments to 120 °C. The Ar flush began with a further increase in temperature to 160 °C and stabilized there. At this temperature the ZnS component grew epitaxially over the CdSe core in 10-min time span. The reaction was quenched by removing the heating mantle, and when the temperature had fallen to around 55 °C (to prevent TOPO from solidifying, 3 ml of butanol was added), 7 ml of anhydrous MeOH was injected into the reaction medium. The nanocrystals formed a precipitate immediately. The precipitate was washed three times with dry MeOH in 5 ml portions and centrifuged in between. The final product was kept under inert atmosphere. Aliquots at different stages of the crystal growth were taken.

**Ligand exchange**—CdSe/ZnS core/shell QDs with excess TOPO were dissolved in chloroform and washed with MeOH four times prior to further processing. The QDs were then dissolved in chloroform and 3-mercaptopropionic acid (0.2 ml, 2.30 mmol) was added via a syringe at room temperature. During a span of three days, 0.1 ml “fresh” mercaptopropionic acid solution was added every day. For the next step, a portion of the material was washed with dry MeOH (3 × 10 ml) to get rid of the unreacted 3-

mercaptopropionic acid, since the QDs precipitated and the unreacted excess acid dissolved and was washed away. Reaction media were kept under nitrogen atmosphere.

**Functionalization with vinyl end-groups**—CdSe/ZnS QDs attached with a mercaptopropionic acid monolayer were dissolved in toluene and reacted with a mixture of 0.01 ml of 7-octenyl dimethyl chlorosilane and 2.0 ml toluene at room temperature producing terminal vinylic end-groups at the surface of the QDs. The system was washed with  $3 \times 5$  ml MeOH with centrifugation between each washing.

**Attaching the ruthenium alkylidene catalyst**—In a vial with septum stopper and nitrogen atmosphere, 0.01 g of ruthenium alkylidene catalyst was dissolved in 2 ml anhydrous dichloromethane. In another vial with a septum stopper and nitrogen atmosphere, the vinyl-functionalized QDs were dissolved in 2 ml anhydrous dichloromethane. Both vials were kept at  $-10$  °C for about 20 min, and the contents of the vials were mixed and allowed to react until they slowly reached room temperature. The material was washed several times with ice-cold MeOH until there was no further color change in the washing solvent, filtered, and dried under vacuum.

**Polymerization of NDC on QDs**—2 ml of anhydrous dichloromethane was added to 0.01 g of the ruthenium “activated” QDs. To this, a mixture of 0.5 ml of trans-3,6-endomethylene-1,2,3,6-tetrahydrophthaloylchloride and 2 ml anhydrous dichloromethane was added. After a couple of minutes, the solution turned dark brown and the viscosity increased. The system was allowed to react for 12 h. To finish the work-up, the QD-polymer was dissolved in chloroform and precipitated in ice-cold MeOH and this cycle was repeated four times. The same procedure was used to synthesize shorter homo-polymer chains with 0.2 ml of the monomer. At the end of the 12-h reaction period, the QD-polymer was dissolved in chloroform and was slowly poured into a beaker containing 15 ml of vigorously stirred ice-cold MeOH. The process of dissolution and precipitation was performed four times. The work-up converted the carbonyl chloride end-groups to methyl esters.

**Co-Polymerization of NDC and norbornoPOSS on QDs**—To 2 ml of dry toluene, 0.01 g of ruthenium “activated” QDs was added. 0.01 g of norbornene-dicarbonyl chloride and 0.046 g of norbornoPOSS (molar ratio of the two monomers was 4:1) were dissolved separately in dry toluene, and added to the vial with the QD-catalyst. Reaction was allowed to proceed at 40 °C for 24 h. After that, the QD-polymer was precipitated with ice-cold MeOH, re-dissolved in toluene, and precipitated in MeOH. This procedure was repeated four times to ensure that there was no unreacted monomer left in the medium. The work-up converted the carbonyl chloride pendant groups to carbonyl methyl esters.

**Polymerization of NDC (free-grown)**—To 3 ml of anhydrous dichloromethane, 0.8 g of trans-3,6-endomethylene-1,2,3,6-tetrahydrophthaloylchloride was added. In a separate vial, 0.001 g of ruthenium alkylidene catalyst was dissolved in 2 ml anhydrous dichloromethane. After mixing the two solutions, the system was allowed to react for 12 h while the viscosity change was observed in the first couple of minutes after mixing. The same procedure was used to synthesize shorter homo-polymer chains, only this time 0.08 g of the monomer was used while the catalyst amount was kept the same. At the end of the 12-h reaction period, the

polymer was dissolved in chloroform and was slowly poured into a beaker containing 15 ml vigorously stirred ice-cold MeOH. The process of dissolution and, consecutively, precipitation was performed four times. The work-up converted the carbonyl chloride pendant groups to carbonyl methyl esters.

**Co-Polymerization of NDC and norbornoPOSS (free-grown)**—To 2 ml anhydrous dichloromethane, 0.03 g norbornoPOSS was added and dissolved completely. 2 ml anhydrous dichloromethane was used to dissolve 0.06 g of trans-3,6-endomethylene-1,2,3,6-tetrahydrophthaloylchloride and 0.001 g ruthenium catalyst separately. Subsequently, these three solutions were mixed and allowed to react for 24 h. At the end of this period, the co-polymer was dissolved in chloroform and slowly poured into a beaker containing 15 ml vigorously stirred ice-cold MeOH. The process of dissolution and precipitation was repeated four times. The process converts the carbonyl chloride pendant groups to carbonyl methyl esters.

**End-capping**—The procedure was performed to cleave off the ruthenium catalyst from the polymer chain ends. The polymer was dissolved in chloroform to which 0.1 ml of vinyl acetate was added. The reaction was allowed to continue for 40 min after which ice-cold MeOH was used to precipitate the polymer. After this, it was dissolved in chloroform and re-precipitated with MeOH and this process was repeated four times.

**Removal of the core/shells**—1 % HF solution in toluene was used overnight to dissolve the inorganic material.

## Conclusions

We were able to synthesize CdSe/ZnS core/shell QDs with narrow size distribution, stable and comparable optical qualities. Our results have shown that we were successful in generating flexible and stable tunable fluorophores with SI-ROMP technique in growing polymer brushes onto CdSe/ZnS in a controlled manner. We were able to grow both homopolymers and co-polymers with different molecular weights and narrow polydispersity directly from the CdSe/ZnS surface. The organic corona was covalently tethered to the QD surface and created distinctive globular features, i.e., finite nanometer-sized structures compared to the amorphous structure in the counterpart of “free” polymer chains. This technique could provide a broadly applicable method to combine the properties of inorganic QDs with a functionalized organic polymer corona in a controlled and pre-determined fashion.

## Acknowledgments

MRH was supported by the US NIH grant R01AI050875.

## References

- Alivisatos AP. Perspectives on the physical chemistry of semiconductor nanocrystals. *J Phys Chem.* 1996a; 100:13226–13239.
- Alivisatos AP. Semiconductor clusters, nanocrystals, and quantum dots. *Science.* 1996b; 271:933.

- Alivisatos AP. Less is more in medicine. *Sci Am.* 2001; 285:66–73.
- Alivisatos P. The use of nanocrystals in biological detection. *Nat Biotechnol.* 2004; 22:47–52. DOI: 10.1038/nbt927 [PubMed: 14704706]
- Banerjee A, Grazon C, Nadal B, Pons T, Krishnan Y, Dubertret B. Fast, efficient, and stable conjugation of multiple DNA strands on colloidal quantum dots. *Bioconj chem.* 2015; 26:1582–1589. DOI: 10.1021/acs.bioconjchem.5b00221
- Bao J, Bawendi MG. A colloidal quantum dot spectrometer. *Nature.* 2015; 523:67–70. DOI: 10.1038/nature14576 [PubMed: 26135449]
- Bhana S, Wang Y, Huang X. Nanotechnology for enrichment and detection of circulating tumor cells. *Nanomedicine.* 2015; 10:1973–1990. DOI: 10.2217/nnm.15.32 [PubMed: 26139129]
- Cao Y, Shi S, Wang L, Yao J, Yao T. Ultrasensitive fluorescence detection of heparin based on quantum dots and a functional ruthenium polypyridyl complex. *Biosens Bioelectron.* 2014; 55:174–179. DOI: 10.1016/j.bios.2013.12.009 [PubMed: 24374300]
- Chan WC, Nie S. Quantum dot bioconjugates for ultra-sensitive nonisotopic detection. *Science.* 1998; 281:2016–2018. [PubMed: 9748158]
- Chen N, et al. Cy5.5 conjugated MnO nanoparticles for magnetic resonance/near-infrared fluorescence dual-modal imaging of brain gliomas. *J Colloid Interface Sci.* 2015; 457:27–34. DOI: 10.1016/j.jcis.2015.06.046 [PubMed: 26151564]
- Cho SH. WE-G-303-00: nanotechnology for imaging and therapy. *Med Phys.* 2015; 42:3693. doi: 10.1118/1.4926080
- Crimmins MT, King BW. An efficient asymmetric approach to carbocyclic nucleosides: asymmetric synthesis of 1592U89, a potent inhibitor of HIV reverse transcriptase. *J Org Chem.* 1996; 61:4192–4193. [PubMed: 11667311]
- Dabbousi BD, et al. (CdSe)ZnS core-shell quantum dots: synthesis and optical and structural characterization of a size series of highly luminescent materials. *J Phys Chem B.* 1997; 101:9463–9475.
- Danek M, Jensen KF, Murray CB, Bawendi MG. Synthesis of luminescent thin-film CdSe/ZnSe quantum dot composites using CdSe quantum dots passivated with an overlayer of ZnSe. *Chem Mater.* 1996; 8:173–180.
- Dawson K, O’Riordan A. Electroanalysis at the nanoscale. *Annu Rev Anal Chem.* 2014; 7:163–181. DOI: 10.1146/annurev-anchem-071213-020133
- Dias EI, Nguyen ST, Grubbs RH. Well-defined ruthenium olefin metathesis catalysts: mechanism and activity. *J Am Chem Soc.* 1997; 119:3887–3897.
- Diaz Fernandez YA, et al. The conquest of middle-earth: combining top-down and bottom-up nanofabrication for constructing nanoparticle based devices. *Nanoscale.* 2014; 6:14605–14616. DOI: 10.1039/c4nr03717k [PubMed: 25208687]
- Duan X, Huang Y, Cui Y, Wang J, Lieber CM. Indium phosphide nanowires as building blocks for nanoscale electronic and optoelectronic devices. *Nature.* 2001; 409:66–69. DOI: 10.1038/35051047 [PubMed: 11343112]
- Ekimov AI, et al. Absorption and intensity-dependent photoluminescence measurements on CdSe quantum dots: assignment of the first electronic transitions. *J Opt Soc Am B.* 1993; 10:100–107.
- Fan XZ, Naves L, Siwak NP, Brown A, Culver J, Ghodssi R. Integration of genetically modified virus-like-particles with an optical resonator for selective bio-detection. *Nanotechnology.* 2015a; 26:205501. doi: 10.1088/0957-4484/26/20/205501 [PubMed: 25915182]
- Fan Y, Liu H, Han R, Huang L, Shi H, Sha Y, Jiang Y. Extremely high brightness from polymer-encapsulated quantum dots for two-photon cellular and deep-tissue imaging. *Sci Rep.* 2015b; 5:9908. doi: 10.1038/srep09908 [PubMed: 25909393]
- Feugang JM, Youngblood RC, Greene JM, Willard ST, Ryan PL. Self-illuminating quantum dots for non-invasive bioluminescence imaging of mammalian gametes. *J Nanobiotechnol.* 2015; 13:38. doi: 10.1186/s12951-015-0097-1
- Fuhrer MS, et al. Crossed nanotube junctions. *Science.* 2000; 288:494–497. [PubMed: 10775104]
- Ganesh N, et al. Enhanced fluorescence emission from quantum dots on a photonic crystal surface. *Nat Nanotechnol.* 2007; 2:515–520. DOI: 10.1038/nnano.2007.216 [PubMed: 18654350]

- Grubbs RH. The development of functional group tolerant ROMP catalysts. *Pure Appl Chem.* 1994; A31:1829–1833.
- Gudiksen MS, Lathon LJ, Wang J, Smith DC, Lieber CM. Growth of nanowire superlattice structures for nanoscale photonics and electronics. *Nature.* 2002; 415:617–620. DOI: 10.1038/415617a [PubMed: 11832939]
- Guyot-Sionnest P, Hines MA. Intraband transitions in semiconductor nanocrystals. *Appl Phys Lett.* 1998; 72:686–688.
- Guzelian AA, Katari JEB, Kadavanich AV, Banin U, Hamad K, Juban E, Alivisatos AP. Synthesis of size-selected, surface-passivated InP nanocrystals. *J Phys Chem.* 1996; 1996:7212–7219.
- Hasan M, Bethel D, Brust M. The fate of sulfur-bound hydrogen on formation of self-assembled thiol monolayers on gold: (1)H NMR spectroscopic evidence from solutions of gold clusters. *J Am Chem Soc.* 2002; 124:1132–1136. [PubMed: 11841257]
- Heath JR, Shiang J. Covalency in semiconductor quantum dots. *J Chem Soc Rev.* 1998; 27:65–71.
- Hines MA, Guyot-Sionnest P. Synthesis and characterization of strongly luminescent ZnS-capped CdSe nanocrystals. *J Phys Chem.* 1996; 100:468–471.
- Hou T, Zhang P, Zhou X, Cao X, Zhao Y. Synthesis of well-defined polymers grafted onto fumed silica by chain exchange reaction and highly pure block copolymers thereby. *Chem Commun.* 2010; 46:7397–7399. DOI: 10.1039/c0cc02135k
- Islam MR, Bach LG, Vo TS, Lee DC, Lim KT. Controlled synthesis, optical properties and cytotoxicity studies of CdSe-poly(lactic acid) multifunctional nanocomposites by ring-opening polymerization. *J Nanosci Nanotechnol.* 2014; 14:6251–6255. [PubMed: 25936098]
- Ivin, KJ., Mol, JC. Olefin metathesis and metathesis polymerization. Academic Press; San Diego: 1997.
- Jiang L, Chen X, Lu N, Chi L. Spatially confined assembly of nanoparticles. *Acc Chem Res.* 2014; 47:3009–3017. DOI: 10.1021/ar500196r [PubMed: 25244100]
- Katari JEB, Colvin VL, Alivisatos AP. X-ray photoelectron spectroscopy of CdSe nanocrystals with applications to studies of the nanocrystal surface. *J Phys Chem.* 1994; 98:4109–4117.
- Klimov VI, McBranch DW, Leatherdale CA, Bawendi MG. Electron and hole relaxation pathways in semiconductor quantum dots. *Phys Rev B.* 1999; 60:13740–13749.
- Labelle AJ, Thon SM, Kim JY, Lan X, Zhitomirsky D, Kemp KW, Sargent EH. Conformal fabrication of colloidal quantum dot solids for optically enhanced photovoltaics. *ACS Nano.* 2015; 9:5447–5453. DOI: 10.1021/acsnano.5b01296 [PubMed: 25880708]
- Lalatsa A, Serrano Lopez DR. Editorial: engineering nanomedicines into safe and effective therapeutics. *Curr Top Med Chem.* 2015; 15:2253. [PubMed: 26043740]
- Lei Y, Wang T, Mitchell JW, Chow LC. Immobilization of xanthate agent on titanium dioxide and surface initiated RAFT polymerization. *J Basic Clin Med.* 2014; 3:1–3. [PubMed: 25717422]
- Levicky R, Koneripalli N, Tirrell M. Concentration profiles in densely tethered polymer brushes. *Macromolecules.* 1998; 31:3731–3734.
- Lynn DM, Kanaoka S, Grubbs RH. Living ring-opening metathesis polymerization in aqueous media catalyzed by well-defined ruthenium carbene complexes. *J Am Chem Soc.* 1996; 118:784–790.
- Manna L, Scher E, Alivisatos PA. Synthesis of soluble and processable rod-, arrow-, teardrop-, and tetrapod-shaped CdSe nanocrystals. *J Am Chem Soc.* 2000; 122:12700.
- Murray CB, Norris DJ, Bawendi MG. Synthesis and characterization of nearly monodisperse CdE (E = S, Se, Te) semiconductor nanocrystallites. *J Am Chem Soc.* 1993; 115:8706–8715.
- Nasilowski M, Spinicelli P, Patriarche G, Dubertret B. Gradient CdSe/CdS quantum dots with room temperature biexciton unity quantum yield. *Nano Lett.* 2015; 15:3953–3958. DOI: 10.1021/acs.nanolett.5b00838 [PubMed: 25990468]
- Nguyen ST, Johnson IK, Grubbs RH, Zeller JW. Ring-opening metathesis polymerization (ROMP) of norbornene by a group VIII carbene complex in protic media. *J Am Chem Soc.* 1992; 114:3974–3975.
- Nguyen ST, Grubbs RH, Zeller JW. Synthesis and activities of new single-component, ruthenium-based olefin metathesis catalysts. *J Am Chem Soc.* 1993; 115:9858–9859.

- Nirmal M, Brus LE. Luminescence photophysics in semiconductor nanocrystals. *Acc Chem Res.* 1999; 32:407–414.
- Pancove, JI. *Dover books on physics.* Dover Publications; New York: 2010. *Optical processes in semiconductors.*
- Peng X, Schlamp MC, Kadavanich AV, Alivisatos AP. Epitaxial growth of highly luminescent CdSe/CdS core/shell nanocrystals with photostability and electronic accessibility. *J Am Chem Soc.* 1997; 119:7019–7029.
- Peng X, Wickham J, Alivisatos AP. Kinetics of II-VI and III-V colloidal semiconductor nanocrystal growth: “focusing” of size distributions. *J Am Chem Soc.* 1998; 120:5343–5344.
- Peng XG, Manna L, Yang WD, Wickham J, Scher E, Kadavanich AV, Alivisatos PA. Shape control of CdSe nanocrystals. *Nature.* 2000; 404:59–61. [PubMed: 10716439]
- Prucker O, Ruhe J. Mechanism of radical chain polymerizations initiated by Azo compounds covalently bound to the surface of spherical particles. *Macromolecules.* 1998a; 31:602–613.
- Prucker O, Ruhe J. Synthesis of poly(styrene) monolayers attached to high surface area silica gels through self-assembled monolayers of azo initiators. *Macromolecules.* 1998b; 31:592–601.
- Samanta A, Banerjee S, Liu Y. DNA nanotechnology for nanophotonic applications. *Nanoscale.* 2015; 7:2210–2220. DOI: 10.1039/c4nr06283c [PubMed: 25592639]
- Schneider M, Fetsch C, Amin I, Jordan R, Luxenhofer R. Polypeptoid brushes by surface-initiated polymerization of N-substituted glycine N-carboxyanhydrides. *Langmuir.* 2013; 29:6983–6988. DOI: 10.1021/la4009174 [PubMed: 23663172]
- Schwab P, Grubbs RH, Ziller JW. Synthesis and application of RuCl<sub>2</sub>(=CHR')(PR<sub>3</sub>)<sub>2</sub>: the influence of the alkylidene moiety on metathesis activity. *J Am Chem Soc.* 1996; 118:100–110.
- Shipway AN, Willner I. Nanoparticles as structural and functional units in surface-confined architectures. *Chem Commun.* 2001; 20:2035–2045.
- Skaff H, Ilker MF, Coughlin EB, Emrick T. Preparation of cadmium selenide-polyolefin composites from functional phosphine oxides and ruthenium-based metathesis. *J Am Chem Soc.* 2002; 124:5729–5733. [PubMed: 12010046]
- Sun D, Tian Y, Zhang Y, Xu Z, Sfeir MY, Cotlet M, Gang O. Light-harvesting nanoparticle core-shell clusters with controllable optical output. *ACS Nano.* 2015; 9:5657–5665. DOI: 10.1021/nn507331z [PubMed: 25933097]
- Talapin DV, Rogach AL, Kornowski A, Haase M, Weller H. Highly luminescent monodisperse CdSe and CdSe/ZnS nanocrystals synthesized in a hexadecylamine-tri-octylphosphine oxide-tri-octylphosphine mixture. *Nano Lett.* 2001; 1:207–211.
- Tenenbaum E, Ben-Dov N, Segal E. Tethered lipid bilayers within porous Si nanostructures: a platform for (optical) real-time monitoring of membrane-associated processes. *Langmuir.* 2015; 31:5244–5251. DOI: 10.1021/acs.langmuir.5b00935 [PubMed: 25902286]
- Tian YC, Newton T, Kotov NA, Guldi DM, Fendler JN. Coupled composite CdS-CdSe and core-shell types of (CdS)CdSe and (CdSe)CdS nanoparticles. *J Phys Chem.* 1996; 100:8927–8939.
- Walba DM, Keller P, Shao R, Clark NA, Hillmyer M, Grubbs RH. Main-chain ferroelectric liquid crystal oligomers by acyclic diene metathesis polymerization. *J Am Chem Soc.* 1996; 118:2740–2741.
- Wang T, Chow LC, Frukhtbeyn SA, Ting AH, Dong Q, Yang M, Mitchell JW. Improve the strength of PLA/HA composite through the use of surface initiated polymerization and phosphonic acid coupling agent. *J Res Natl Inst Stand Technol.* 2011; 116:785–796. [PubMed: 22399838]
- Wang W, et al. Photoligation of an amphiphilic polymer with mixed coordination provides compact and reactive quantum dots. *J Am Chem Soc.* 2015; 137:5438–5451. DOI: 10.1021/jacs.5b00671 [PubMed: 25797052]
- Weller H. Colloidal semiconductor Q-particles: chemistry in the transition region between solid state and molecules. *Angew Chem Int Ed Engl.* 1993; 32:41–53.
- Wijesena RN, Tissera N, Kannangara YY, Lin Y, Amaratunga GA, de Silva KM. A method for top down preparation of chitosan nanoparticles and nanofibers. *Carbohydr Polym.* 2015; 117:731–738. DOI: 10.1016/j.carbpol.2014.10.055 [PubMed: 25498694]

- Wu Z, Nguyen ST, Grubbs RH, Zeller JW. Reactions of ruthenium carbenes of the type  $(PPh_3)_2(X)_2Ru = CH-CH = CPh_2$  ( $X = Cl$  and  $CF_3COO$ ) with strained acyclic olefins and functionalized olefins. *J Am Chem Soc.* 1995; 117:5503–5511.
- Yenice Z, Schon S, Bildirir H, Genzer J, von Klitzing R. Thermoresponsive PDMAEMA brushes: effect of gold nanoparticle deposition. *J Phys Chem B.* 2015; 119:10348–10358. DOI: 10.1021/acs.jpcc.5b04757 [PubMed: 26132296]
- Zhang Y, Wang TH. Quantum dot enabled molecular sensing and diagnostics. *Theranostics.* 2012; 2:631–654. DOI: 10.7150/thno.4308 [PubMed: 22916072]
- Zhang L, Zhao D. Applications of nanoparticles for brain cancer imaging and therapy. *J Biomed Nanotechnol.* 2014; 10:1713–1731. [PubMed: 25992438]
- Zhao S, Liu H. Bottom-up nanofabrication through catalyzed vapor phase HF etching of  $SiO_2$ . *Nanotechnology.* 2015; 26:015301. doi: 10.1088/0957-4484/26/1/015301 [PubMed: 25474677]

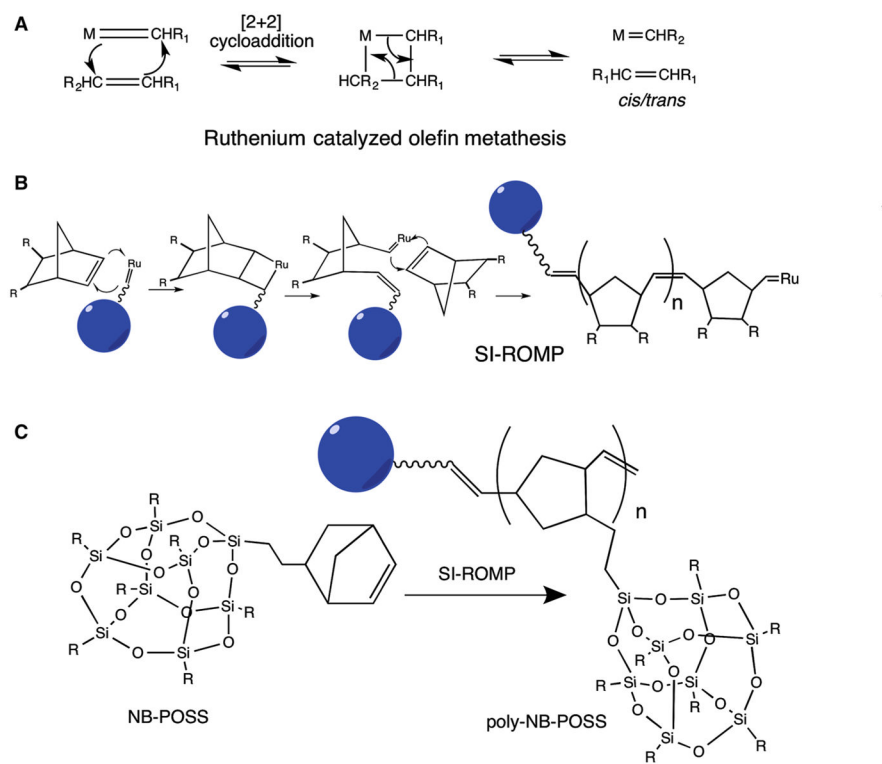


**Fig. 1.** Reaction schemes for synthesis of polymer-coated QDs by SI-ROMP. **a** Ruthenium-catalyzed olefin metathesis, **b** SI-ROMP using norbornene-dicarbonyl chloride (R = COCl) to give a homo-polymer, and **c** SI-ROMP using norbornenoPOSS (R = isobutyl) to give a homo-polymer

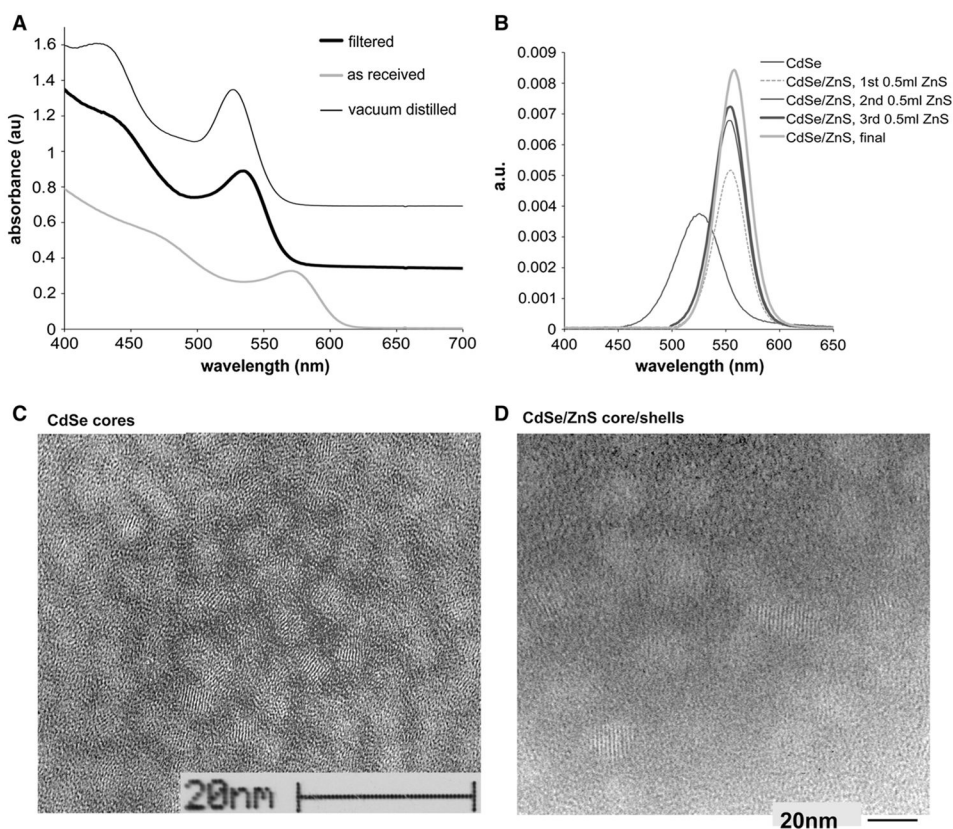


**Fig. 2.**  
**a** UV-vis spectra of CdSe cores prepared from Cd(CH<sub>3</sub>)<sub>2</sub> precursors either as received, filtered, or vacuum distilled. Curves are vertically offset for clarity. **b** Photoluminescence emission of CdSe cores (prepared from filtered Cd(CH<sub>3</sub>)<sub>2</sub>) after sequential additions of ZnS to shells. The shell evolution is observed through taking aliquots from the reaction medium after subsequent addition of the shell component while the final spectrum is after full work-up. **c, d** TEM micrographs of **c** CdSe and **d** CdSe/ZnS QDs. The average size of CdSe QDs ranges from 3.5 to 4 nm, with a lattice spacing of 3.5 Å observed by fringes. ZnS shell growth resulted in an average size ranging from 4.5 to 5 nm and lattice fringes at 3.5 Å still observed

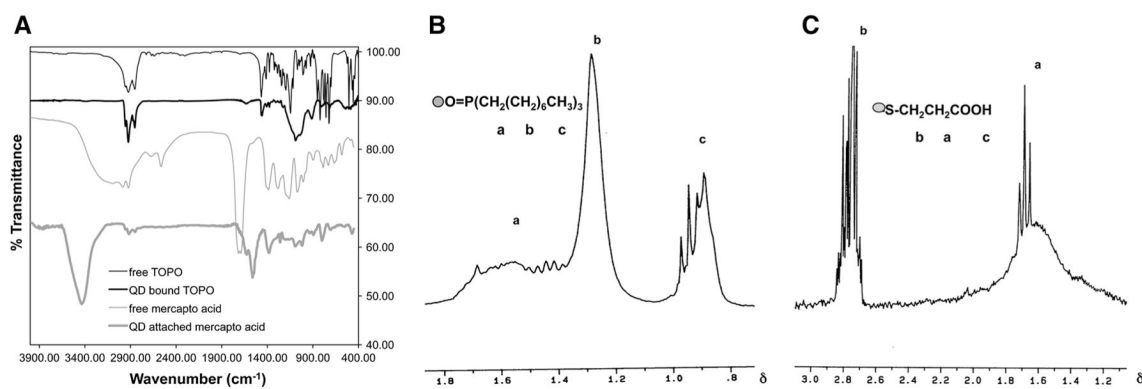


**Fig. 3.** **a** FT-IR of QD-attached mercaptopropionic acid, free mercaptopropionic acid, free TOPO, and QD-bound TOPO. Curves are offset vertically for clarity. **b–c** Proton NMR of **b** QD-attached TOPO (**a** 1.49–1.67 $\delta$ , **b** 1.26–1.46 $\delta$ , **c** 0.88–0.96 $\delta$ ) and **c** QD-attached mercaptopropionic acid (**a** 1.65–1.71 $\delta$ , **b** 2.68–2.83 $\delta$ , **c** 11.70 $\delta$ )

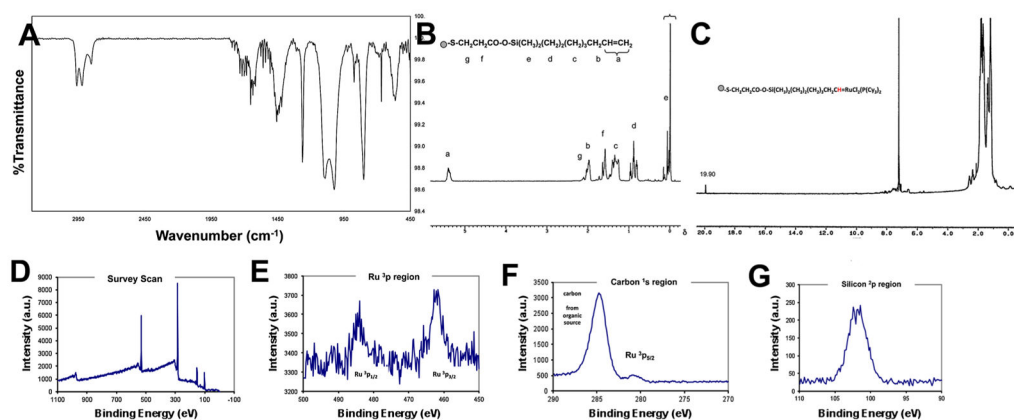


**Fig. 4.** **a** FT-IR of QD-octenyl with terminal double bonds. **b** Proton NMR of QD-octenyl with terminal double bonds (**a** 5.37–5.39 $\delta$ , **b** 1.96–1.98 $\delta$ , **c** 1.27–1.39 $\delta$ , **d** 0.78–0.95, **e** 0.05–0.32 $\delta$ , **f** 1.65–1.71 $\delta$ , **g** 2.68–2.83 $\delta$ ). **c** Proton NMR of QD-sequestered ruthenium alkylidene catalyst (alkylidene proton 19.90 $\delta$ , –Si(CH<sub>3</sub>)<sub>2</sub> protons 0.07–0.34 $\delta$ , QD-SCH<sub>2</sub> protons 2.69–2.84 $\delta$ , the rest of the protons are convoluted in the 0.97–2.20 $\delta$  region, whereas in free ruthenium alkylidene catalyst the alkylidene proton appears at 20.62 $\delta$  with the two  $\alpha$  protons of the benzene ring showing up at 8.73 $\delta$ ). **d–g** XPS spectra of QDs sequestered with the ruthenium catalyst: **d** Survey scan, **e** ruthenium region, **f** carbon region, and **g** silicon region

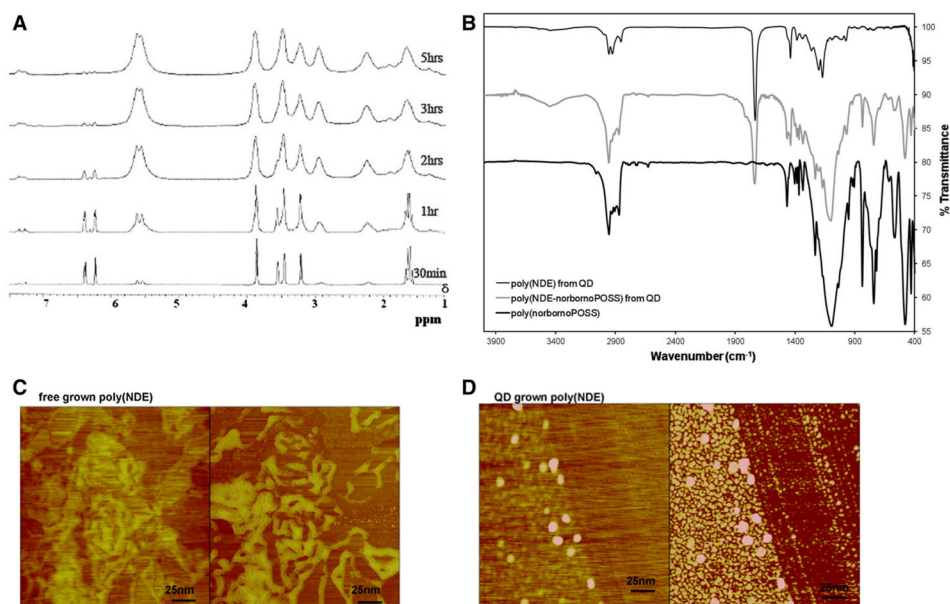


**Fig. 5.** **a** In situ  $^1\text{H}$  NMR of poly(NDC) formation from the QD surface. **b** FT-IR of QD-grown poly(NDE), poly(NDE–norbornoPOSS), and free-grown poly(norbornoPOSS). Curves are vertically offset for clarity. **c, d** AFM image of **c** free-grown poly(NDE) versus **d** QD-grown poly(NDE). All images are taken in AFM tapping mode and show both the height (*left image*) and phase (*right image*). **c** Neat polymer at the edge of drying front with normal polymer morphology—only amorphous agglomerations of various sizes. **d** Individual polymer covered QDs at the edge of drying front all with the relatively same size, 50 nm in diameter

**Table 1**

Summary of thermal characterization of the polymers

	MW (GPC)	PD (GPC)	T <sub>g</sub> (°C) (DSC)	T <sub>d</sub> (°C) (TGA)	T <sub>m</sub> (°C) (DSC)
QD-grown and recovered polymer					
Poly(NDE)	8000	1.2	86	413	-
Poly(NDE)	264,000	1.4	94	415	-
Poly(NDE-norbornoPOSS)	15,000	1.8	77	431	-
Free-grown polymer					
Poly(NDE)	195,000	1.3	90	420	-
Poly(NDE)	525,000	1.4	100	420	-
Poly(NDE-norbornoPOSS) (4:1 ratio)	280,000	1.7	88	427	-
Poly(norbornoPOSS)	34,000	1.6	44	447	-